arXiv:astro-ph/0007447v2 31 Jan 2001

On the compared accuracy and reliability of spectroscopic and photometric redshift measurements

Alberto Fernández-Soto[1,2,3], Kenneth M. Lanzetta[1], Hsiao-Wen Chen[4], Sebastian M. Pascarelle[1], and Noriaki Yahata[1]

ABSTRACT

We present a comparison between the catalog of spectroscopic redshifts in the Hubble Deep Field (HDF) recently published by Cohen and collaborators and the redshifts that our group has measured for the same objects using photometric techniques. This comparison is performed in order to fully characterize the errors associated to the photometric redshift technique. The compilation of spectroscopic redshifts incorporates previously published results, corrections to previously published wrong values, and new data, and includes over 140 objects in the HDF proper. It represents the deepest, cleanest, most complete spectroscopic catalog ever compiled. We particularly study each and every object for which our redshift and the one measured by Cohen and collaborators seem to disagree. In most of those cases the photometric evidence we put forth is strong enough to call for a careful review of the spectroscopic values, as the spectroscopic values seem to be in error. We show that it is possible to characterize the systematic errors associated to our technique, which when combined with the well-measured photometric errors allow us to obtain complete information on the redshift of each galaxy and its associated confidence interval, regardless of its apparent magnitude. One of the main conclusions of this study is that, to date, all the redshifts from our published catalog that have been checked have been shown to be correct (within the stated confidence limits). This implies that our set of spectrophotometric galaxy templates is a fair representation of the galaxy population at all redshifts ($0 < z < 6$) and magnitudes ($R < 24$) explored to date. On the other hand, spectroscopy of faint sources is subject to unknown and uncharacterized systematic errors. These errors will in turn be transmitted to any photometric redshift technique which uses spectroscopic samples in its calibration. Our analysis proves that photometric redshift techniques can and must be used to extend the range of applicability (in redshift, signal-to-noise, and apparent magnitude) of the spectroscopic redshift measurements.

Subject headings: Cosmology: Observations — Galaxies: Distances and Redshifts — Methods: data Analysis — Techniques: Photometric — Techniques: Spectroscopic

1. INTRODUCTION

Measuring redshifts of extragalactic objects through spectroscopy is a hard task. This is particularly true in those extreme cases when the available technology is strained to its limits and applied to objects which are faint and consequently offer low signal-to-noise spectra. Even in cases where a good signal-to-noise ratio is achieved, the absence of clear and characteristic features in the observed spectral range can hamper

[1]Department of Physics and Astronomy, State University of New York at Stony Brook,
Stony Brook, NY 11794-3800, U.S.A. (fsoto, lanzetta, sam, nyahata@sbastr.ess.sunysb.edu)

[2]Osservatorio Astronomico di Brera, Via Bianchi 46, Merate (LC), I-23807, ITALY

[3]Marie Curie Fellow

[4]The Observatories of the Carnegie Institution of Washington, 813 Santa Barbara Street, Pasadena, CA 91101, U.S.A. (hchen@ociw.edu)

the observer's ability to determine a trustworthy redshift. Moreover, the process of line identification which is necessary in order to measure a redshift is very often too subjective, and hence likely to be biased. In order to avoid this problem, various techniques have been developed that try to automate the process, amongst them the application of spectral cross-correlation, principal component analysis, and combinations thereof—see for example Glazebrook, Offer, & Deeley (1998). However, these methods still suffer from numerous problems produced by low signal-to-noise spectra, instrument-related systematics, or inability to handle samples covering large redshift ranges.

A completely orthogonal approach consists in the use of purely photometric information on the objects under study. In this approach, the weight of the redshift identification is carried by the broad-band continuum shape and the presence/absence of spectral breaks, such as the one at 4000 Å, or the onset of the Lyman α forest and the Lyman limit at high redshifts, rather than by narrow-band emission/absorption features. Photometric redshift methods like these have been known and used for many years—for example by Butchins (1981), Loh & Spillar (1986), or Connolly et al. (1995)—but the interest in them has grown enormously since the Hubble Space Telescope (HST) produced the Hubble Deep Field (HDF) observations (Williams et al. 1996). The reason for this interest is that the HDF observations are ideally suited for the application of photometric redshift techniques: they include multiband information spanning all of the visible and near-IR range and they are extremely deep [reaching to AB(8140) $\approx$ 29]. This second fact also implies that it is utterly impossible to obtain spectra of the bulk of the detected objects, and given the extremely high density of galaxies it is even difficult sometimes to measure the spectra of the (relatively) bright ones.

Since the data became available in December 1995, several papers have been published giving spectroscopic redshifts of over a hundred objects in the HDF [see references in Cohen et al. (2000), hereafter C00]. Several groups have also published the results of different photometric redshift techniques applied to the field, with catalogs of photometry and photometric redshifts: Lanzetta, Yahil, & Fernández-Soto (1996) (LYF96 hereafter), Gwyn & Hartwick (1996), Sawicki, Lin, & Yee (1997), Wang, Bahcall, & Turner (1998), Fernández-Soto, Lanzetta, & Yahil (1999) (FLY99 hereafter), Furusawa et al. (2000), Benítez (2000). At least one comparison of photometric and spectroscopic redshifts has been published (Hogg et al. 1998), with "photometrists" supplying answers to the questions of the "spectroscopists," who compared the former's results with the ones measured from their spectra. This comparison showed that photometric techniques, as a whole, can give relatively accurate measurements (to within $\Delta z/(1+z) \approx 0.10$ rms), and that they are very well suited for the analysis of large samples of deep, multi-color imaging data.

However, it is not so well known that photometric redshift techniques have also been instrumental in detecting some incorrect spectroscopic redshifts. Our group made public as early as 1997 a list of "successes" and "failures" of our photometric redshift technique, in which it was shown that many of the discordances observed in the HDF $z_{\rm phot}$ vs $z_{\rm spec}$ plots could actually be due to mistakes in the spectroscopic redshifts—and some of them certainly were, as acknowledged by the respective observers afterwards [see Lanzetta, Fernández-Soto, & Yahil (1998) for details]. Apparently, it has not been sufficiently remarked that detecting and identifying the narrow features which are necessary to unambiguously determine a spectroscopic redshift is a very hard task in the low S/N spectra we are confronting.

Another proof of the quality of the photometric redshifts is the fact that a number of objects for which our own group measured redshifts $z_{\rm phot} > 5$ have been observed with the Keck telescope, and confirmed to be amongst the most distant objects ever observed. For example, Spinrad et al. (1998) measured $z_{\rm spec} = 5.34$ for object #3 in FLY99 ($z_{\rm phot} = 5.28$), and Weymann et al. (1998) measured $z_{\rm spec} = 5.60$ for object #213 in the same catalog ($z_{\rm phot} = 5.64$).

Recently, Cohen and collaborators have published a complete list of spectroscopic redshifts in the HDF and flanking fields (C00). They have compiled all the data published to date, eliminated and/or ammended the redshifts that have been shown to be in error, and added a number of observations of their own. Their final list includes 671 entries, 158 of which are within the

HDF proper (we have moved nine objects which are located in the PC from their "flanking fields" table to the HDF table). After excluding 11 stars and 1 object (HDF36774_1235) which does not lie inside the area we studied, we are left with 146 galaxies using which both methods are compared.

In this paper, the catalog of spectroscopic redshifts compiled by Cohen et al. (2000) is compared to the catalog of photometric redshifts obtained by our group. Cohen's catalog is the deepest (reaching down to $R = 24$ and beyond), most complete (92% complete to that limit) and cleanest (at least seven redshifts have been corrected from previously published values which were shown to be in error) ever published. By performing this comparison on a sample of bright objects—where the photometric uncertainties are small—we expect to obtain a complete characterization of the systematic errors associated with our technique, and hence to be able to measure accurate errors associated to any of our photometric redshift determinations. A first comparison shows that over 90% of the residuals are well represented by a gaussian distribution with an rms dispersion $\sigma_{\Delta z/(1+z)} \lesssim 0.08$ at all redshifts. Nine objects out of 146 have residuals which are more than $4\sigma_{\Delta z/(1+z)}$ away from the spectroscopic value. A very interesting result comes from the detailed analysis of these nine objects with discordant redshifts: we show in this paper that *at least* five of the discordant points can be due to errors in the *spectroscopic* values, with the proportion being possibly as high as 90% (eight out of nine). In the only case in which the photometric redshift technique is responsible for the discordance, we show that when the full redshift likelihood function and the systematic errors—as estimated from the whole sample—are taken into account, the spectroscopic redshift is in fact *well within* 2σ *of the photometric redshift.*

These results lead us to conclude that the spectroscopic redshift technique is plagued by unknown and uncharacterized errors, which become problematic, or even dominant, when low signal-to-noise spectra are analysed. These errors are then transmitted to those photometric redshift techniques that make use of spectroscopic redshifts as "calibrators." On the other hand, the photometric redshift technique we have presented in FLY99 has *as of today* not been shown to be in error over the stated confidence limits in a single case, and has the advantage of including a full characterization of its errors, through the use of the redshift likelihood function.

Our experience shows that, as a general rule, the systematic errors dominate our technique for objects down to $m = m_{\rm lim} - 2$, where $m_{\rm lim}$ is the detection limit in the images. This means that, for HDF-style surveys, redshifts can be obtained with $\sigma_{\Delta z/(1+z)} \lesssim 0.08$ for objects down to $AB \approx 26$, two magnitudes below the limits attainable by traditional spectroscopy with the largest telescopes. For magnitudes fainter than this limit, the photometric errors dominate over the systematic ones, and the errors associated with the photometric redshift become larger. In both cases the accuracy of the method should remain constant, as long as our set of template spectral energy distributions (SEDs) remains a fair representation of the observed galaxy population. This has been proven to be the case at all redshifts ($0 < z < 6$) and magnitudes ($R < 24$) probed to date. This paper further proves that there is a strict upper limit (less than 5.4%, to 2σ confidence) to the possible percentage of galaxies whose SEDs differ significantly (within the available photometry) from our templates in a flux limited ($R < 24$) sample.

The structure of this paper is as follows: In §2 we present the data. Section 3 introduces the comparison, and in §4 we fix our attention on the objects for which the spectroscopic and photometric redshifts disagree. Section 5 presents the data on one particular object which does not show up as "discordant" but for which we are led to believe the spectroscopic redshift is in error. In §6 we discuss our results and in §7 we enumerate our conclusions.

2. THE COMPARISON REDSHIFT CATALOG

In this Section we present the photometric and spectroscopic catalogs used in the comparison, and the process of cross-identification of the objects in both lists.

2.1. The Spectroscopic Redshift Catalog

The sample of spectroscopic redshifts is the one given in C00. It contains 671 entries and is, as stated by the authors, complete to over 92% for objects inside the HDF area to $R = 24$, irre-

spective of morphology. Some fainter objects are also included. All spectroscopy involved was performed using LRIS on the Keck Telescopes. It is very important to note that this is *the cleanest, deepest, most complete* list of spectroscopic redshifts available for the HDF, which is to say, the cleanest, deepest, most complete sample of spectroscopic redshifts available to date.

The authors of C00 also remark that all redshifts listed have been carefully checked. In this process several values have been changed from previously published papers: six objects from Cohen et al. (1996), two objects from Steidel et al. (1996), two objects from Phillips et al. (1997), and an unspecified number of objects from Hogg et al. (1998) and the Hawaii web database[5]. As explained in §1, some of these changes were actually induced by comparison of the original spectroscopic values and the photometric redshifts as supplied by ourselves and other groups. The final list includes 146 objects with reliable spectroscopic measurements: the 149 listed in Table 2b of C00, plus nine objets from their Table 2a—Flanking Fields—that lie within the PC and, hence, enter our analysis, minus 11 stars, and minus one object (HDF36377_1235) which does not lie in the area studied by us (see footnote about this object in Section 2.3).

2.2. The Photometric Redshift Catalog

Our photometric redshift sample is basically the one published in FLY99. We used the photometric catalog as described in that paper, but we applied to it the more accurate photometric redshift technique described in Yahata et al. (2000) (Y00 hereafter). The main difference with respect to the FLY99 paper is the inclusion of two starburst spectrophotometric templates, which improves the behavior of our method in the redshift range $z = 2.0 - 4.0$ (where our former method systematically underestimated the redshifts by $\Delta z \approx 0.5$), as demonstrated by Benítez (2000). We have also decreased the calculation step from $\delta z = 0.04$ to $\delta z = 0.01$, to take full profit of the excellent quality of the measurements.

It must be remarked that *the objective of our technique is not to fit the observed photometry*, but to obtain a best-fit measurement of the redshift. It is important to notice that in the case of bright objects our fit will never be a "perfect fit" (the photometry being too accurate for our sample of SEDs to reproduce every possible spectrum) whereas, in the opposite end, for very faint objects any basically correct SED will represent an equally good fit to the observations. Hence, the particular value of the maximum likelihood (or the value of the minimum χ^2) cannot be taken as a measurement of the goodness of the estimated redshift.

The sample includes 1067 galaxies, with photometric redshifts spanning the range $z \approx 0 - 6$, and is complete to $AB(8140) = 26.0$ over 5.2 square arcminutes and to $AB(8140) = 28.0$ over 3.9 square arcminutes. The general properties of the redshift distribution as outlined in FLY99 do not change in any major way with the use of the new templates, but for the already mentioned correction of the systematic problem between $z = 2$ and $z = 4$. As a reference, it must be remarked that FLY99 was also a refinement of our previous work, LYF96, written at a time when the infrared images were not yet available.

2.3. Cross-Identification of Objects in Both Catalogs

To match objects in both catalogs, we cross-correlate the coordinates and compare apparent magnitudes, which proves to be sufficient to unequivocally pair 98% of the objects in the spectroscopic redshift catalog with objects in the photometric redshift catalog. Only in three cases was it necessary to use the redshift information, as two objects with different photometric redshifts were being associated to a single object in the C00 list. In these cases (see Table 1) the object whose photometric redshift was closer to the observed spectroscopic redshift was taken to be the counterpart. It may be claimed that this method will produce a slight bias favoring the goodness of the comparison. It must be remarked, though, that in these cases the position listed by C00 (and supposedly in that case, the position of the center of the slit when the observations were made) is actually half way in between the two objects in our catalog, which are in every case approximately equally bright. Under these circumstances, the decision as to which object is the one actually observed can only depend on extra information, the best available to us being precisely the one given by the

[5] `http://www.ifa.hawaii.edu/~cowie/tts/tts.html`

photometric redshift. Table 2 lists the complete cross-identifications.

The two objects listed by C00 as coming from Stern & Spinrad (1999) have very clear counterparts in our catalog. In fact, both of them were actually passed by ourselves to the authors as objects with $z \approx 5$ to be observed with Keck. Their positions as listed by C00, though, differ from the positions in our catalog by more than 1 arcsecond, and needed to be matched individually after the original cross-identification.

For the sake of completeness, we also include in Table 3 the objects listed in Table 10 of C00. These are the only objects with $R < 24$ for which the authors could not determine a redshift, although they have spectra of quality comparable to others in the sample. Their magnitudes range between $R = 23.2$ and $R = 24.0$. One of them (HDF36526_1202) does not have a counterpart in our FLY99 catalog. After careful checking we have discovered that this object (for which we measured its photometry and redshift, see Table 4) did not enter the final published version of the catalog, although it fulfills all the positional and brightness criteria that we used. Another object listed in Table 10 of C00 (HDF36378_1235) does not lie in the area we studied, so it is not included in our Table.[6]

The final comparison catalog includes 146 objects with reliable spectroscopic and photometric redshifts.

3. COMPARISON OF PHOTOMETRIC AND SPECTROSCOPIC REDSHIFTS

In this section we present a direct comparison of redshift estimates based on spectroscopic and photometric methods for all 146 objects in the combined catalog. This is, to the best of our knowledge, the most accurate comparison ever performed of the two techniques for this kind of deep sample, because it includes *all* the spectroscopic redshifts available, as obtained by several groups of observers using the largest telescopes in operation, over a period of over four years, and with several values retracted and/or ammended when known to be in error. Moreover, as the authors of C00 remark, the redshifts given in their tables are not *"preliminary values,"* but *"final redshifts."*

Table 2 and Figures 1 and 2 show the comparison of the redshifts assigned by the spectroscopic and photometric methods to 146 objects in the HDF.

We used a 4σ-clipping algorithm to measure the dispersion between the redshift values measured with both techniques—with a sample of 146 objects, the probability of having one $> 4\sigma$ discordant point by chance is less than 1% for a normal distribution. Our statistic of choice is $\Delta z/(1+z) = (z_{\rm phot} - z_{\rm spec})/(1+z_{\rm spec})$. When the sample is taken as a whole (146 objects), the mean value is $\langle \Delta z/(1+z) \rangle = 0.0035$, with rms dispersion $\sigma_{\Delta z/(1+z)} = 0.065$, and nine objects having discordant redshifts—over the four sigma level. When we break the sample into three subsamples ("low" redshift from 0.0 to 1.5 with 113 objects, "medium" redshift from 1.5 to 4.0 with 27 objects, and "high" redshift from 4.0 to 6.0 with 6 objects), the respective mean values are $\langle \Delta z/(1+z) \rangle = 0.0010$, 0.0160, and -0.0045[7]. The rms dispersions are $\sigma_{\Delta z/(1+z)} = 0.063$, 0.076, and 0.016, and the numbers of discordant points are, respectively, 7, 2, and 0. All these values are tabulated in Table 5. Figure 3 shows that the distribution of the residuals, except for the $> 4\sigma$-discordant points mentioned above, is very well represented by a gaussian. It also supports the choice of a 4σ value for the clipping algorithm.

The first immediate result from this comparison confirms what was known previously: careful enough photometric redshift techniques, when applied to data of good enough quality (in terms of accurate photometry and realistic error estimates), are able to measure redshifts to an accuracy better than $\sigma_{\Delta z/(1+z)} \approx 0.10$, with less than 10% of the measurements being discordant. In fact, *in a first assessment* our particular application of these techniques reaches an accuracy bet-

[6] This object has—to less than 0.5 arcseconds and 0.1 magnitudes—the same position and brightness of the object mentioned in the previous subsection as the one whose coordinates put it out of the HDF as defined by us, which *does have a redshift* ($z = 0.485$). It is one of the objects added as a "note added in proof" by Cohen and collaborators, which may explain this apparent mistake.

[7] Notice that there is an observational "void" in the spectroscopic redshift distribution with no objects with $1.355 < z_{\rm spec} < 1.980$. Objects at redshifts $1.0 - 1.4$ and $2.0 - 2.5$ are well represented in our sample, though

ter than $\sigma_{\Delta z/(1+z)} \approx 0.08$ over the whole observed range ($z = 0$ to $z = 6$), with less than 7% discordances. This result is in perfect agreement with our previously published estimates in FLY99 and Y00.

When assessing the errors associated to the photometric redshift measurements, we must take into account that they are twofold: on one side, the fact that we are using a discrete, finite, set of SEDs will produce a systematic error, as obviously not all galaxies (in fact, *no galaxy*) can be exactly represented by them. We refer to this source of systematic error as "cosmic variance", and it is most important in the bright regime, when photometric errors are negligible. On the other hand, when very faint galaxies are studied, the cosmic variance becomes negligible and the errors in the photometric redshift induced by the uncertainties in the galaxy photometry dominate the error budget. The photometric component of the error can be assessed using the likelihood function, as the photometric uncertainties are included in its calculation. The assessment of the systematic errors, however, must be attained by the comparison of photometric and accurate, reliable, spectroscopic redshifts for a suitably large sample of bright galaxies—where the photometric errors will not dominate. In order to ensure that we have such a sample, we study in the next section the objects in our catalog that show discordances larger than 4σ.

4. THE DISCORDANT 7%: A BLIND TEST OF SPECTROSCOPIC REDSHIFTS

In this section we present in detail the available data for the nine objects that show discordant redshifts in the photometric and spectroscopic catalogs. The photometric data include the fluxes in 7 bands (HST F300W, F450W, F606W, and F814W; and ground-based J, H, and K), from which our photometric redshift technique yields the estimated redshifts, best-fit galaxy types, and redshift likelihood functions. Regarding the spectroscopic data, we have looked at the original sources of publication whenever available, and studied carefully the spectra presented. Most of the objects scrutinized in this section, however, are new additions by Cohen and collaborators who do not present the spectra in their paper.

Together with a brief discussion on each object, we also present in Figure 4 the photometric data (filled points with vertical error bars indicating the 1-σ errors and horizontal error bars showing each filter FWHM). The figure also shows in the central panel our best-fit spectrum obtained by taking the best-fit redshift and type, and applying the H I absorption as described in LYF96 and FLY99, the fluxes expected from our best-fit spectrum through all seven filters (empty circles), and the redshift likelihood function for each object. In the top panels we show the spectra of our six galaxy templates (corresponding from left to right and top to bottom to E/S0, Sbc, Scd, Irr, SB1 and SB2, see FLY99 and Y00) redshifted to the spectroscopic redshift and with the effect of intergalactic H I absorption added. In most cases, that is the best approximation to the "observed spectrum" we can get.

Thumbnail F814W images of the objects with discordant redshifts are presented in Figure 5. Table 6 presents all the relevant information about each of these objects.

Before entering the individual discussions, we would like to remark on two important facts regarding the expected nature of the errors in both methods. First, the spectroscopic redshifts must be extremely precise by their own nature—to within $\sigma_z \approx 0.001$ for low-medium resolution spectroscopy (C00 quote $\approx$ 200 km s^{-1} as "typical uncertainty"). In case of error, it would be due to misidentification of absorption and/or emission features, and the redshift values should not show any particular regularity and/or concentration. On the other hand, photometric redshifts have a built-in lack of precision due to the broad-band nature of the features analysed. This leads to a rms dispersion of (in our case) $\sigma_{\Delta z/(1+z)} \lesssim 0.08$. In this case, however, the confusion between different redshifts is fully characterized by the known colors of the redshifted templates, and the likelihood of any redshift value will always be reflected in the likelihood function—as long as the collection of SEDs used in the analysis really covers all possible spectral types. These considerations lead us to the following assertions:

a) When the redshifts obtained by both techniques disagree, but the likelihood function

shows a secondary peak at (or near) the value of $z_{\rm spec}$, then it is most likely that the spectroscopic redshift is correct. Detailed analysis of the likelihood function must be performed in these cases in order to obtain a "confidence interval" around the photometric redshift value and, if still necessary, discover the origin of the discordance.

b) When there is no secondary peak in the likelihood function at (or near) the value suggested by the spectroscopy, and there are spectral features that match the redshift measured by the photometric redshift technique, it is most likely that the photometric redshift is correct. In this case, the spectroscopic redshift may be wrong due to misidentification of spectral features.

c) When both techniques disagree and there is no hint either in the spectrum or in the likelihood function about which one is wrong, all the evidence must be produced and the possible causes for the disagreement analyzed. These include, but are not limited to: observational errors (like misassignment of spectra to objects), presence of nearby objects that may alter the accuracy of the photometry or send light into the slit during spectroscopy, and the possibility of the object belonging to a spectral class not included in the photometric templates (*e.g.* a QSO or a star).

With these ideas in mind, we start the individual study of all nine objects with discordant redshifts. Where no explicit information is given about the original source of the spectroscopic redshifts, they came from Cohen and collaborators' new data. We follow here the naming convention that assigns the name HDFXXXXX_YYYY to the object with coordinates (J2000) $12^h XX^m XX^{\rm s}.X$, $+62^\circ YY'YY''$.

4.1. HDF36386_1234

This is an object of magnitude $R = 24.04$. The spectroscopic redshift is 0.904, and is listed as having quality class 9, which means it has been assigned a redshift based solely on a *"single strong absorption feature, assumed to be 2800 Å because of the shape of the continuum"* [see Cohen et al. (1999) for a full description of the spectroscopic quality classes used by the authors]. This means that a strong absorption at approximately 5330 Å must be the only clear spectroscopic feature of this object.

Our technique assigns to this object (number 727 in FLY99) a redshift of 0.15. It is clear from Figure 4 that the very low flux in the F300W band is very difficult to reconcile with the shape of the rest of the spectrum if the galaxy is at $z \approx 0.9$. This fact reduces the likelihood of $z \approx 0.9$ to negligible values. On the other hand, to explain the 5330 Å feature using our redshift we would have to identify it with the G band, which would assign to this object a redshift $z \approx 0.24$, or with Hβ at $z \approx 0.10$. Both would be perfectly in line with our typical dispersion, but this identification is not at all definitive.

As can be observed in Figure 5, there is a nearby object in projection on the sky, less than three arcseconds away. The redshift of this object is (C00) $z_{\rm spec} = 0.944$. We cannot discard the possibility of confusion between both objects.

Summing up, we consider this object *unlikely* to be at the suggested $z_{\rm spec} = 0.904$ due to its SED, but cannot present evidence conclusive enough to definitively prove that the photometric value $z_{\rm phot} = 0.15$ is right.

4.2. HDF36396_1230

This is a very interesting object. According to C00, it is a *"broad-line AGN"*, given that its brightness ($R = 24.4$ at $z_{\rm spec} = 0.943$) corresponds to only a few times L^*, too low to be a QSO. It is also identified as the brightest object in the peak (cluster?) of the redshift distribution at $z \approx 0.96$. It is assigned spectroscopic quality 7, which indicates *"only one broad emission line, assumed to be 2800 Å"* (which means it lies at ≈ 5440 Å in the observer's frame). In Figure 4 we show the spectrum of an average QSO template (Chen 2000, private communication) instead of all six galaxy templates at $z = z_{\rm spec}$, to take its claimed nature into account. Cohen *et al.* also mention in Section 3 of their paper that they did not include this object in their *"blind check of photometric redshifts"* because *"none of the groups came close to predicting [its] redshift"*.

As can be seen immediately, the SED of a QSO

at $z = 0.943$ looks *absolutely different* from what is observed in this case. This fact alone leads us to claim that the likelihood of this object being a $z = 0.943$ QSO is negligible. The likelihood function shows that the case of either a normal or a starbursting galaxy at the same redshift can also be discarded with the same level of security—unless the spectrum is a pathological case, and cannot be represented by any "normal", "starburst", or QSO spectrum, the redshift is unlikely to be $z \approx 0.94$. Figure 5 shows that our photometry should not be contaminated by bright nearby neighbors.

If we study now our photometric redshift (object number 688 in FLY99), we find a perfect agreement for the SED with one corresponding to a Scd galaxy at redshift $z_{\rm phot} = 3.40$. At this redshift, the Lyman α line would be redshifted to 5350 Å.

Combining the width of the peak in our likelihood function with the detection (as indicated by C00) of a strong emission line at $\lambda \approx 5440$ Å, and the presence of a strong break in the flux of the object at approximately the same wavelength, we are led to interpret this object as being a normal galaxy at $z \approx 3.475$, in perfect agreement with our estimate. We cannot elaborate on the broad component of the emission line with the data available to us.

4.3. HDF36409_1205

This is yet another object of spectral quality class 9, with spectroscopic redshift $z_{\rm spec} = 0.882$ and magnitude $R = 22.94$. It is listed by C00 as having appeared for the first time in C96, but we have not been able to locate it in that reference. The absorption feature putatively identified by C00 as MgII 2800 must be at $\lambda = 5270$ Å. Figure 4 shows a case very similar to that of HDF36386_1234: there is an obvious lack of flux in the F300W filter, that renders unlikely—in our analysis—the $z \approx 0.9$ interpretation.

With our photometric redshift technique, we obtain an excellent fit to the SED of this object for a $z_{\rm phot} = 0.00$ Scd galaxy. The only tentative interpretation of the observed spectrum that is consistent with this is the observed absorption feature corresponding to Mg I absorption at $z = 0.02$.

Once again in this case, we are forced to conclude that the spectroscopic suggested value $z_{\rm spec} = 0.882$ is *unlikely* to be the true redshift, but we have no other strong evidence to support our case for $z_{\rm phot} = 0.00$ either. Moreover, it can be seen in Figure 5 that this object lies in a particularly crowded region of the sky, which makes the case all the more difficult.

4.4. HDF36414_1143

This object is listed in C00 as having magnitude $R = 23.52$ and redshift $z_{\rm spec} = 0.548$. Quality class is 3, meaning *"multiple features, faint, id uncertain"*.

Looking at Figure 4 we see that the SED does not fit any type of galaxy at this redshift, and that our interpretation of it as a Scd galaxy at redshift $z_{\rm phot} = 1.32$ is, while better, not optimal. One possible reason for this is that this object (number 200 in FLY99, $AB(8140) = 23.19$) actually overlaps in the sky with another *brighter* object (number 183 in FLY99, $AB(8140) = 22.42$) with a spectroscopic redshift listed in C00 as $z_{\rm spec} = 0.585$. The distance between the centers of both objects is only 2 arcseconds.

If confusion caused by the proximity of the second object is not the issue here, then we should try to identify some of the features described by C00 with absorption features at approximately $z = 1.32$. If, for example, Cohen and collaborators had identified an absorption feature as Ca II (H,K) at $z = 0.548$ (which would put it at $\lambda \approx 6120$ Å), it could also be Mg II at $z \approx 1.19$. *Mutatis mutandis*, the G band at $z = 0.548$ could also be identified as Mg II at $z \approx 1.38$.

As a resume, once again we have to admit that we have no clear explanation as to which is the reason for the discordance in this case, if not the possibility of confusion induced by the vicinity of another bright object.

4.5. HDF36441_1410

This object was first presented in Lowenthal et al. (1997)(L97 hereafter). Its R magnitude is 24.26, and the listed redshift is $z_{\rm spec} = 2.267$. C00 assesses it as a "secure" redshift, while Lowenthal and collaborators classify it as "definite." The authors of L97 kindly published their spectra in Figure 2 of their paper, so we can assess by ourselves the quality of the spectrum.

Our analysis assigns to this object a redshift of 0.01. It can be seen in Figure 4 that the fit to the SED at the spectroscopic redshift is very good using a SB1 type, in fact (to the eye) comparable to the fit to the SED redshifted to our photometric value. The difference, though, is given by the F606W and F814W bands having tiny error bars, so the weight of the likelihood function is driven by them and their better fit to the photometric value. This can of course be appreciated from the fact that there is no secondary peak in the likelihood function near the spectroscopic value.

After a first look at Figures 4 and 5 nothing seems to be wrong with the spectroscopic value, and we actually counted this object as one of our failures in FLY99. Nevertheless, encouraged by the general success of our technique and piqued by the absence of a secondary peak at $z \approx z_{\rm spec}$, we tried to find the expected features of a $z \approx 0.01$ galaxy in the observed spectrum as presented in L97.

We then found the following: the emission line identified in L97 as Lyman α can actually be identified with [O II] 3727 at $z = 0.065$. In that case, the Calcium doublet should be observed at λ=4190,4228 Å, the G absorption band should be at λ =4580 Å, and the Na I absorption feature should be observed at λ =6278 Å. All these features can be observed in the spectrum with *at least* the same level of significance of most of the original identifications. Lowenthal and collaborators considered this identification as a possibility in their paper (see Appendix in L97), and decided from the implied luminosity and equivalent width of the putative [O II] line that it was "not implausible."

It should also be noticed that the presence of a continuum break expected at the position of the Lyman α line as identified in L97 (which would be identified as the 4000 Å break according to the photometric redshift) cannot be checked in the spectrum, because it would lie at the very blue end of it. Also, the slope of the UV spectrum seems too steep for a typical $z \approx 2$ galaxy, as can be seen by comparing it with other spectra in the same figure in L97.

Our conclusion about this object is that the photometric value fits better all the available evidence, including the spectrum itself. The spectroscopic value is likely to be in error due to misidentification of features in a noisy spectrum.

4.6. HDF36478_1256

This is another object described originally in L97. It has $z_{\rm spec} = 2.931$ and $R = 24.35$. The spectroscopic quality is 2 (*"good with multiple features"*) in C00, and "definite" in the original reference. As can be seen in the top panels of Figure 4, its SED can be almost perfectly fitted by an Irr galaxy at the spectroscopic redshift, with the only slight caveat being the presence of detectable but faint ($\approx 3\sigma$) flux in the F300W filter.

In a very similar fashion to the previous case, our photometric method prefers a lower redshift solution at $z_{\rm phot} = 0.26$. As above, the break in the spectrum which corresponded to the onset of the Lyman α forest using the redshift value from L97 is then taken to be the 4000 Å break.

However, detailed observation of our likelihood function shows that there is a second peak at $z \approx 3$. The secondary peak actually reaches a maximum at $z = 3.13$, with a value which is almost 20% of the maximum at $z = 0.26$.

Following our previously stated considerations, we deem our technique gives us in this case an incorrect answer, as the spectroscopic evidence agrees within the errors with a secondary peak in the likelihood function. Nevertheless, when the likelihood function is used to perform a complete assessment of the errors in $z_{\rm phot}$, it shows the value $z = 2.931$ to be "within the errors": the 1σ interval around $z_{\rm phot}$ is 0.15–0.38, the 2σ interval is 0.06–0.52 *plus* 2.80–3.49.

4.7. HDF36494_1317

This object is listed in C00 as having $z_{\rm spec} = 0.271$, with a magnitude $R = 23.63$ and a quality assessment of 3.

Figure 4 shows that, while there is no way that a redshift 0.271 SED can fit the observed photometry, a perfect fit is achieved by using a Scd spectral template at $z_{\rm phot} = 1.24$.

A footnote in C00 refers to this object with the following text: *"Definite emission line at 8340 Å, possible emission line at 6363 Å. If both are real,* $z = 0.271$. *If only the stronger one is real, then* $z = 1.238$. *Spectrum too red to reach 3727 Å if* $z = 0.271$."

With this information in hand, we consider we can peacefully rest our case. The redshift of the

galaxy is perfectly well measured to be $z = 1.238$, in exact agreement with our technique.

4.8. HDF36561_1330

An object with $z_{\rm spec} = 0.271$, $R = 23.80$, and spectral quality 4. Figure 4 shows that a fit can be obtained at that redshift for the photometry, though the goodness-of-fit is not comparable with the one obtained using the photometric redshift technique.

The photometric redshift is $z_{\rm phot} = 1.07$, with the likelihood function excluding any other possibility for the redshift.

In this case, as in the previous one, a footnote in C00 adds more information: *"Emission line at 8340 Å is interpreted as Hα. Spectrum too red to reach 3727 Å if $z = 0.271$."*

As in the previous case, we think that the observed line must be identified as being O II 3727 at a redshift $z = 1.238$, which will be in agreement with our photometric measurement to $\approx 8\%$ error in $\Delta z/(1+z)$.

4.9. HDF36569_1302

This object is listed in C00 as having magnitude $R = 23.84$, redshift $z_{\rm spec} = 0.474$, and spectral quality 1 (*"secure redshift, multiple features identified"*). In Figure 4, though, we see that the spectrum is much too bright in the IR bands, and that none of the SEDs can actually fit the observations when redshifted to that value. Examination of Figure 5 allows us to discard the possibility of any nearby IR-bright object interfering with our measurements.

Our photometric redshift technique suggests a value of 1.27, with a spectral type Sbc. No secondary peaks are apparent in the likelihood function. However, we have tried to cross-identify the possible features that the observers may have identified to be at $z = 0.474$, and found no way to position them on a $z \approx 1.27$ spectrum.

Careful observation of the circumstances is thus required. A look at Figure 5 shows that this object is close ($< 3.5''$) to a very bright ($R = 21.07$) galaxy, number 458 in FLY99, already observed with Keck by C96 and the Hawaii group. This bright galaxy has a spectroscopic redshift of 0.475, as listed in C00, and has an SED which is utterly different from the one of HDF36569_1302. No sign of interaction or merging is visible, which could be used to explain the same redshift being assigned to both objects.

We are led to conclude in this case that the spectroscopic redshift is in error due to confusion with a nearby bright source. Given that the only evidence left is the photometry, and that our technique has shown to be right in over 95% of the cases, we conclude that the redshift of this object must be (within errors) $z = 1.27$.

5. AN EXTRA POSSIBLY WRONG SPECTROSCOPIC REDSHIFT

We present in this Section the photometric and spectroscopic data for an extra object. Although in this case the redshift difference is not over 4σ (our stated criterium to define "discordance"), we have good reasons to believe the spectroscopic value may be in error.

The object in question is HDF36450_1251. It is completely isolated (see Figure 5), and C00 lists for it a redshift $z_{\rm spec} = 2.801$ and a magnitude $R = 24.37$. The authors of C00 assign to the spectrum a quality flag 3, which means there are multiple identified features, but their identification is uncertain.

One problem springs immediately into view when looking at Figure 4—the object has an 11σ detection in the F300W image, where zero flux would be expected from an object at such a high redshift. Our photometric technique suggests a lower redshift $z_{\rm phot} = 2.23$. The SED fits perfectly, and the likelihood function admits quite a wide range of values, essentially between $z = 2.1$ and $z = 2.3$. The F300W detection makes the likelihood of the object being at any $z > 2.6$ completely negligible.

We conclude in this case that the redshift assigned by the spectroscopic method cannot be right due to serious discordance with the observations.

6. DISCUSSION

We have presented in this paper a detailed comparison of the cleanest, deepest and most complete catalog of spectroscopic redshifts available for the HDF with our catalog of photometric redshifts. The first result of the comparison is that

the photometric redshifts are accurate to within $\Delta z/(1+z) = 0.08$ (rms) *at all redshifts explored between* $z = 0$ *and* $z = 6$. The fraction of *apparently* discordant points is 6.2%. This fraction, when taken in separate redshift intervals, amounts to 6.2% at $z = 0.0-1.5$ (7 objects out of 113), 7.4% at $z = 1.5 - 4.0$ (2 objects out of 27), and 0% at $z > 4.0$ (out of six objects).

We have performed a careful study of all the available evidence regarding the discordant redshifts. This analysis has resulted in the following:

- In five out of nine cases, we have evidence that indicates that *the spectroscopic redshifts are in error.* The causes for this range from misidentification of spectral features in noisy spectra to confusion with nearby objects.
- Only in one of the nine discordant cases we have concluded that the photometric value is not correct. A full study of the errors associated with the value $z_{\rm phot}$, though, shows that the spectroscopic and photometric values *do agree* to within a 2σ confidence level.
- In three cases the evidence we have gathered is not enough to decide which of the techniques is giving more accurate results. We kindly ask from these lines the authors of C00 to produce the evidence, to help in deciding on these cases.

Once this analysis is fully taken into account, the final figures for the accuracy of our redshift determination technique become the following: The rms dispersions in $\Delta z/(1+z)$ at low, medium, and high redshift are $\sigma_{\Delta z/(1+z)} = 0.063$, 0.068, and 0.016, with mean values $\langle \Delta z/(1+z) \rangle = 0.0003$, 0.0186, and -0.0045, and discordant fractions 0%, 0% (*outside the quoted error bars*), and 0%. The total number of points in each redshift bin are 109, 26, and 6, respectively. All these final values are also tabulated in Table 5, and presented in Figures 6 and 7.

This result shows that *at most* three out of 146 galaxies can have SEDs which are not well represented in our template set. Even in the case that in all three cases the photometric redshifts were shown to be in error, and that these errors were exclusively caused by the incompleteness of our SED sample (leaving aside other possible systematic effects induced by variance of HI absorption along different sightlines or other problems that may be inherent to our likelihood technique), this would set a stringent limit to the percentage of galaxies which are not well represented by our templates. Applying Poisson statistics to these figures, we get that such a percentage cannot be (to a 2σ confidence level) larger than 5.4%, and will be smaller (and possibly zero) if any or all of those three uncertain cases are shown to be caused by errors in the spectroscopic measurements. This result holds also when the putative presence of extra dust in the observed spectra is taken into account. We detect no evidence in our analysis for the presence of highly-reddened galaxies whose SEDs cannot be reproduced with our templates (which, being observational in origin, *do* contain some amount of dust).

We can use this sample of photometric and spectroscopic redshifts to characterize the errors associated with our technique. A full description of this procedure will be presented elsewhere, but we describe here the operational steps necessary to measure the confidence intervals for any particular object. As was stated in the Introduction, and also in Lanzetta, Fernández-Soto, & Yahil (1998) and Y00, the photometric redshift error has two components. The first one is induced by photometric uncertainty in the measurement of the fluxes, dominates at the faint end, and is fully taken into account by the use of the likelihood function. The second one is systematic, due to cosmic variance, and can be characterized by a typical dispersion measured from a sample of bright objects, where the photometric error is negligible. Using the sample we have just presented, we estimate (as a zero-th order approximation) this dispersion to be constant in $\Delta z/(1+z)$, and equal to $\sigma_{\Delta z/(1+z)} = 0.065$.

In order to combine both error components, we can convolve the redshift likelihood function with a gaussian with a variable $\sigma_G(z) = (1+z) \times \sigma_{\Delta z/(1+z)}$. In doing this we are assuming that the systematic error follows a normal distribution, which was tested in Section 3. The resulting function can be normalized to yield a redshift probability density, which can be used following the standard methods to calculate confidence intervals. In those cases where the probability density is multimodal—as is the case with HDF36478_1256—the confidence inter-

vals may also be multimodal, *i.e.* disjoint. This procedure, when applied to the particular case of HDF36478_1256, yields the above stated confidence limits (0.15–0.38, 1σ) (0.06–0.52 *plus* 2.80–3.49, 2σ). In most bright objects, though, the redshift likelihood function shows a single, sharp peak. In these cases the convolution with the gaussian will obviously produce a curve that is very approximately gaussian, and the confidence limits will approximately coincide with those given by the value of $\sigma_G(z)$ used.

It is a very remarkable fact that our technique has an "error rate" of 0% (in number of confirmed wrong redshifts compared to total), which cannot be higher than 2% even if all three dubious cases prove to be wrong. In comparison, the spectroscopic technique error rate is *at least* 3.4% (even when only *"definitive"* redshifts, as published by C00, are taken into account, and assuming all three undefined discordant redshifts have correct values of $z_{\rm spec}$), and it can be as high as 14.3% or higher (when all the HDF spectroscopic values that have been published and then retracted are included, together with those objects which have been observed but for which a spectroscopic redshift has been impossible to measure).

7. CONCLUSIONS

We have shown that our photometric redshift technique produces accurate measurements to $\Delta z/(1+z) \lesssim 0.07$ (rms) at all redshifts $0 < z < 6$. We have also shown that in every case where there is a large difference between carefully measured spectroscopic redshifts and carefully measured photometric redshifts, and the systematic and photometric errors are included in the analysis, the spectroscopic redshift is the one in error (although in a few cases we have no evidence to prove either one to be right). In fact, the proportion of incorrect spectroscopic redshifts *even after careful double-checking of all the data involved* is $\approx 3\%$ and, depending on how they are counted, it may be as high as 14%. On the other hand, in the single studied case where the photometric value seems to be incorrect, the analysis of the likelihood function shows that the real redshift value is indeed within the errors given by the photometric method.

One conclusion we extract from this result is that our set of spectral energy distribution templates is a fair, complete, dense representation of all the galaxy spectral distributions that have been observed to date. We can confirm that in the bright limit, where the photometric errors can be ignored—this applies in the case of the HDF to all galaxies for which spectroscopy is available—the errors in $\Delta z/(1+z)$ are dominated by the systematics and are *at all redshifts* $\lesssim 0.07$ (rms). This paper further proves that there is a strict upper limit (less than 5.4%, to 2σ confidence) to the possible percentage of galaxies whose SEDs differ significantly from our templates in a flux limited ($R < 24$) sample. This limit is calculated by applying Poisson statistics to the fact that *at most three galaxies out of 146* may have redshifts which disagree with our measurements to a significant (more than 4σ) level.

In the limit of bright objects the likelihood function (which by its nature only includes the photometric information) has to be convolved with an (assumed) gaussian distribution with the above calculated $\sigma_{\Delta z/(1+z)}$ in order to account for the systematic errors and to obtain realistic errors. In the faint limit, where the photometric errors dominate, the likelihood function by itself represents a good assessment of the errors—although, of course, it must also be convolved with the same gaussian in order to include the systematic component.

There is an important conclusion that can be extracted from this work that affects other photometric redshift techniques. Some of the methods that have been put forward [*e.g.* Wang, Bahcall, & Turner (1998); Connolly et al. (1995); Csabai et al. (2000)] are based on the use of a "calibrating sample" of redshifts, which are taken to be perfectly measured. Using this sample a set of parameters is determined that gives the most accurate possible reproduction of the observed spectroscopic redshifts, and then these parameters are used to calculate redshifts of objects which do not have spectroscopic values. One of the most popular versions of this method uses polynomial fits to define a "redshift vs observed colors" function [like in Wang, Bahcall, & Turner (1998) and Connolly et al. (1995)]. Another possibility is to iteratively "tune" or "improve" the galactic spectral templates to minimize the dispersion in the $z_{\rm phot}$ versus $z_{\rm spec}$ plane [this is the method followed

by Csabai et al. (2000)]. *Both these techniques, as well as any other using similar methods, are extremely sensitive to errors in the spectroscopic sample.* By their own nature they will try to "absorb" any outlier point into the fit, hence improving the "formal" fit at the price of distorting the real underlying relation, and predicting wrong redshifts for any point with similar colors to the ones in error.

It is obvious that the spectroscopic redshift technique has limits in apparent magnitude and/or signal-to-noise ratio where problems arise. Our analysis shows that by magnitude $AB(8140) \approx 24$ even the best instruments available produce spectra that are susceptible to line misidentification, even when carefully analyzed by expert observers. Our photometric redshift technique, on the other hand, has proved its accuracy and reliability for all redshifts $0 < z < 6$ and magnitudes $R < 24$ that have been observed. This allows us to obtain an accurate and detailed measurement of the systematic errors associated to it. Together with the likelihood function—which measures for each individual galaxy the errors induced by the photometric uncertainties—and assuming that our set of spectrophotometric templates is complete (which has been verified for all cases observed to date), our photometric redshift technique has the advantage over traditional spectroscopy of giving *complete information* on the measured redshift *and* its associated error.

We hence conclude that our photometric method is both accurate (within its stated errors) and reliable, and that it is in fact more accurate and reliable than the spectroscopic method when analyzing faint galaxy data.

We thank Judy Cohen and her collaborators, as well as all the other groups involved in spectroscopy of HDF objects, for making their results public. We also thank Bob Williams and his team at STScI for providing us with the HDF images, Mark Dickinson for making the IR Kitt Peak images available, and an anonymous referee for useful suggestions that have improved the paper. A.F.S. acknowledges support from a European Union Marie Curie Fellowship. K.M.L., S.M.P., and N.Y. were supported by NASA grant NAGW-4422 and NSF grant AST-9624216. During the preparation of this paper we have made extensive use of NASA's ADS Abstract Service, the LANL archive, and the NASA/IPAC Extragalactic Database (NED) which is operated by the Jet Propulsion Laboratory, California Institute of Technology, under contract with NASA.

REFERENCES

Benítez, N. 2000, ApJ, 536, 571

Butchins, S. A. 1981, A&A, 97, 407

Cohen, J. G., Cowie, L. L., Hogg, D. W., Songaila, A., Blandford, R., Hu, E. M., & Shopbell, P. 1996, ApJ, 471, L5

Cohen, J. G., Hogg, D. W., Pahre, M. A., Blandford, R., Shopbell, P., & Richberg, K. 1999, ApJS, 120, 171

Cohen, J. G., Hogg, D. W., Blandford, R., Cowie, L. L., Hu, E., Songaila, A., Shopbell, P., & Richberg, K. 2000, ApJ, 538, 29 (C00, also `astro-ph/9912048`)

Connolly, A. J., Csabai, I., Szalay, A. S., Koo, D. C., Kron, R. G., & Munn, J. A. 1995, AJ, 110, 2655

Csabai, I., Connolly, A. J., Szalay, A. S., & Budavári, T. 2000, AJ, 119, 69

Fernández-Soto, A., Lanzetta, K. M., & Yahil, A. 1999, ApJ, 513, 34 (FLY99)

Furusawa, H., Shimasaku, K., Doi, M., & Okamura, S. 2000, ApJ, 534, 624

Glazebrook, K., Offer, A. R., & Deeley, K. 1998, ApJ, 492, 98

Gwyn, S. D. J., & Hartwick, F. D. A. 1996, ApJ, 468, L77

Hogg, D. W., *et al.* 1998, AJ, 115, 1418

Lanzetta, K. M., Yahil, A., & Fernández-Soto, A. 1996, Nature, 381, 759 (LYF96)

Lanzetta, K. M., Fernández-Soto, A., & Yahil, A. 1998, in Proc. STScI 1997 May Symp., The Hubble Deep Field, ed. M. Livio, S. M. Fall, & P. Madau (Cambridge: Cambridge University Press)

Loh, E. D., & Spillar, E. J. 1986, ApJ, 303, 154

Lowenthal, J. D., *et al.* 1997, ApJ, 481, 673 (L97)

Phillips, A. C., Guzmán, R., Gallego, J., Koo, D. C., Lowenthal, J. D., Vogt, N. P., Faber, S. M., & Illingworth, G., D. 1997, ApJ, 489, 543

Sawicki, M. J., Lin, H., & Yee, H. K. C. 1997, AJ, 113, 1

Spinrad, H., Stern, D., Bunker, A., Dey, A., Lanzetta, K. M., Yahil, A., Pascarelle, S., & Fernández-Soto, A. 1998, AJ, 116, 2617

Steidel, C. C., Giavalisco, M., Dickinson, M., & Adelberger, K. L. 1996, AJ, 112, 352

Stern, D., & Spinrad, H. 1999, PASP, 111, 1475

Wang, Y., Bahcall, N., & Turner, E. L. 1998, AJ, 116, 2081

Weymann, R. J., Stern, D., Bunker, A., Spinrad, H., Chaffee, F. H., Thompson, R. I., & Storrie-Lombardi, L. J. 1998, ApJ, 505, L95

Williams, R. E., *et al.* 1996, AJ, 112, 1335

Yahata, N., Lanzetta, K. M., Chen, H.-W., Fernández-Soto, A., Pascarelle, S., Yahil, A., & Puetter, R.C. 2000, ApJ, 538, 493 (Y00)

This 2-column preprint was prepared with the AAS LaTeX macros v5.0.

TABLE 1

OBJECTS WITH DOUBLE CROSS IDENTIFICATIONS IN THE CATALOGS[a]

Cohen *et al.* 2000				Fernández-Soto *et al.* 1999					θ[b]
RA(−12h)	Dec(−62°)	$z_{\rm spec}$	R	ID	RA(−12h)	Dec(−62°)	$z_{\rm phot}$	$AB(8140)$	(arcsec)
36:49.95	12:25.9	1.205	23.71	353	36:49.95	12:25.4	1.07	24.32	0.5
				363	36:49.99	12:26.3	0.01	24.43	0.5
36:52.86	14:08.2	3.367	24.49	957	36:52.99	14:08.5	3.48	26.85	1.0
				959	36:52.91	14:08.5	0.04	26.32	0.5
36:57.51	12:12.1	0.561	22.62	7	36:57.60	12:12.4	0.71	23.16	0.7
				6	36:57.45	12:11.9	0.91	23.28	0.5

[a]The first object listed in each pair was taken as the identification

[b]Distance between the position in C00 and FLY99

TABLE 2

COMPARISON OF BOTH CATALOGS

Cohen *et al.* 2000				Fernández-Soto *et al.* 1999					
RA(−12h)	Dec(−62°)	$z_{\rm spec}$	R	ID	RA(−12h)	Dec(−62°)	$z_{\rm phot}$	$AB(8140)$	$\Delta z/(1+z)$[a]
36:38.43	12:31.2	0.944	22.87	716	36:38.40	12:31.32	0.70	22.61	−0.13
36:38.61	12:33.8	0.904	24.04	727	36:38.60	12:33.86	0.15	23.93	−0.40*
36:38.99	12:19.7	0.609	22.14	617	36:38.96	12:19.77	0.54	22.21	−0.04
36:39.60	12:30.2	0.943	24.40	688	36:39.56	12:30.49	3.40	25.40	1.26*
36:40.02	12:07.3	1.015	22.75	466	36:40.00	12:07.38	0.93	22.28	−0.04
36:40.85	12:03.1	1.010	23.49	402	36:40.81	12:03.05	0.98	23.36	−0.01
36:40.94	12:05.3	0.882	22.94	424	36:40.95	12:05.36	0.00	23.28	−0.47*
36:41.24	12:02.9	3.220	23.94	390	36:41.23	12:02.93	3.51	24.03	0.07
36:41.34	11:40.8	0.585	21.91	183	36:41.33	11:41.01	0.75	22.42	0.10
36:41.43	11:42.5	0.548	23.51	200	36:41.39	11:43.01	1.32	23.19	0.50*
36:41.62	11:31.7	0.089	19.36	85	36:41.61	11:31.82	0.10	19.76	0.01
36:41.62	12:00.5	0.483	25.03	365	36:41.59	12:00.57	0.23	24.88	−0.17
36:41.70	12:38.7	2.591	24.32	702	36:41.71	12:38.82	2.40	24.60	−0.05
36:41.95	12:05.4	0.432	20.82	391	36:41.93	12:05.43	0.50	21.01	0.05
36:42.04	13:21.2	0.846	23.95	902	36:42.02	13:21.47	0.93	23.59	0.05
36:42.71	13:06.7	0.485	22.02	817	36:42.72	13:07.13	0.68	22.19	0.13
36:42.93	12:16.4	0.454	20.51	467	36:42.91	12:16.37	0.45	20.73	−0.00
36:43.16	12:42.2	0.849	22.34	694	36:43.15	12:42.23	0.72	21.74	−0.07
36:43.21	11:48.1	1.010	23.10	195	36:43.18	11:47.99	1.11	22.45	0.05
36:43.42	11:51.4	1.242	23.00	228	36:43.40	11:51.57	0.98	23.05	−0.12
36:43.61	12:18.1	0.752	22.56	465	36:43.62	12:18.28	0.64	22.71	−0.06
36:43.81	11:42.9	0.765	21.26	122	36:43.79	11:42.88	0.64	20.87	−0.07
36:43.92	12:40.5	4.540	26.00	674	36:43.84	12:41.54	4.45	25.00	−0.02
36:43.97	12:50.1	0.557	20.84	720	36:43.96	12:50.07	0.54	20.97	−0.01
36:44.07	14:09.8	2.267	24.26	1062	36:44.07	14:10.05	0.01	24.63	−0.69*
36:44.10	13:10.7	2.929	23.84	815	36:44.09	13:10.75	3.18	24.03	0.06
36:44.19	12:40.3	0.875	23.39	650	36:44.18	12:40.35	0.92	23.33	0.02
36:44.20	12:47.8	0.555	21.40	709	36:44.18	12:47.83	0.54	21.62	−0.01
36:44.38	11:33.2	1.050	21.96	17	36:44.37	11:33.15	0.96	21.26	−0.04
36:44.49	11:42.3	1.020	24.30	99	36:44.45	11:42.17	0.96	22.71	−0.03
36:44.61	13:04.6	0.485	21.14	774	36:44.58	13:04.62	0.67	21.22	0.12
36:44.64	12:27.4	2.500	23.66	517	36:44.63	12:27.42	2.47	23.73	−0.01
36:44.67	11:49.2	4.580	26.00	173	36:44.65	11:50.45	4.53	25.04	−0.01
36:44.83	12:00.1	0.457	22.85	270	36:44.82	12:00.22	0.36	22.99	−0.07
36:45.01	12:39.6	1.225	24.53	625	36:44.99	12:39.63	1.18	23.89	−0.02
36:45.03	12:51.0	2.801	24.37	712	36:45.02	12:51.02	2.23	24.08	−0.15*
36:45.36	11:53.5	2.799	22.53	175	36:45.34	11:52.74	3.20	23.24	0.11
36:45.36	13:46.8	3.160	25.15	964	36:45.35	13:47.00	3.19	25.09	0.01
36:45.41	13:25.8	0.441	22.33	876	36:45.40	13:25.97	0.46	22.61	0.01
36:45.86	13:25.7	0.321	20.71	869	36:45.85	13:25.87	0.41	20.93	0.07
36:45.86	14:11.9	2.427	24.85	1054	36:45.88	14:12.10	2.41	25.21	−0.00
36:45.88	11:58.3	5.600	27.00	213	36:45.89	11:58.26	5.65	27.17	0.01
36:45.96	12:01.3	0.679	23.88	247	36:45.95	12:01.40	0.76	23.72	0.05
36:46.13	12:46.5	0.900	22.86	653	36:46.12	12:46.50	0.59	22.36	−0.16
36:46.17	11:42.2	1.013	21.52	45	36:46.16	11:42.09	1.04	21.26	0.01
36:46.34	14:04.6	0.962	21.69	1018	36:46.35	14:04.68	0.85	21.24	−0.06
36:46.50	14:07.5	0.130	23.87	1029	36:46.53	14:07.60	0.16	23.95	0.03
36:46.51	11:51.3	0.503	22.00	124	36:46.50	11:51.33	0.41	21.99	−0.06
36:46.51	12:03.5	0.454	24.32	245	36:46.54	12:03.12	0.50	24.35	0.03
36:46.80	11:44.9	1.060	24.23	50	36:46.86	11:44.84	1.06	23.23	0.00
36:46.95	12:26.1	2.969	25.13	444	36:46.92	12:26.07	2.69	25.24	−0.07
36:47.00	12:36.9	0.321	20.62	537	36:47.03	12:36.86	0.47	20.98	0.11
36:47.10	12:12.5	0.677	24.63	318	36:47.07	12:12.52	0.75	24.82	0.04
36:47.16	14:14.4	0.609	23.92	1048	36:47.18	14:14.24	0.69	23.55	0.05
36:47.17	13:41.7	1.313	23.93	917	36:47.17	13:41.88	1.16	23.72	−0.07
36:47.28	12:30.7	0.421	22.63	476	36:47.28	12:30.68	0.47	22.77	0.03
36:47.55	12:52.7	0.681	24.26	671	36:47.54	12:52.68	0.75	23.93	0.04
36:47.75	12:55.7	2.931	24.35	687	36:47.77	12:55.68	0.26	23.95	−0.68*
36:47.79	12:32.9	0.960	23.80	483	36:47.78	12:32.94	1.03	23.34	0.04
36:48.07	13:09.0	0.476	20.43	751	36:48.07	13:09.02	0.38	20.45	−0.07
36:48.27	14:17.1	2.005	23.58	1044	36:48.32	14:16.61	2.49	23.40	0.16
36:48.29	14:26.3	0.139	18.70	1067	36:48.32	14:26.25	0.11	19.18	−0.03
36:48.33	11:46.0	2.980	24.58	21	36:48.29	11:45.91	3.17	25.07	0.05

TABLE 2—*Continued*

Cohen *et al.* 2000				Fernández-Soto *et al.* 1999					
RA(−12h)	Dec(−62°)	$z_{\rm spec}$	R	ID	RA(−12h)	Dec(−62°)	$z_{\rm phot}$	$AB(8140)$	$\Delta z/(1+z)$[a]
36:48.33	12:14.3	0.962	23.87	297	36:48.25	12:13.91	1.12	22.55	0.08
36:48.62	13:28.1	0.958	23.14	838	36:48.62	13:28.23	1.06	22.74	0.05
36:48.77	13:18.4	0.753	22.87	780	36:48.78	13:18.45	0.79	22.69	0.02
36:48.98	12:45.8	0.512	23.48	565	36:48.99	12:45.89	0.53	23.66	0.01
36:49.05	12:21.1	0.953	22.59	339	36:49.05	12:21.24	0.85	22.44	−0.05
36:49.24	11:48.8	0.961	23.26	18	36:49.24	11:48.49	0.99	22.95	0.01
36:49.34	11:55.1	0.961	23.36	79	36:49.33	11:55.05	0.95	23.43	−0.01
36:49.36	13:11.2	0.477	21.97	743	36:49.37	13:11.25	0.45	22.12	−0.02
36:49.43	13:16.5	0.271	23.63	759	36:49.44	13:16.65	1.24	23.23	0.76*
36:49.43	13:46.8	0.089	17.97	914	36:49.44	13:46.91	0.06	18.16	−0.03
36:49.49	14:06.6	0.752	21.95	989	36:49.50	14:06.75	0.91	21.80	0.09
36:49.57	12:20.0	0.961	24.40	319	36:49.51	12:20.10	0.93	24.41	−0.02
36:49.63	12:57.6	0.475	21.91	655	36:49.63	12:57.57	0.46	21.99	−0.01
36:49.70	13:13.0	0.475	21.46	746	36:49.71	13:13.04	0.54	21.45	0.04
36:49.72	14:14.9	1.980	23.18	1016	36:49.82	14:14.99	1.64	23.40	−0.11
36:49.80	12:48.8	3.233	25.13	568	36:49.81	12:48.79	3.50	25.18	0.06
36:49.86	12:42.3	0.751	24.38	506	36:49.86	12:42.20	0.96	24.47	0.12
36:49.95	12:25.9	1.205	23.71	353	36:49.94	12:25.44	1.07	24.32	−0.06+
36:50.09	14:01.0	2.237	24.55	960	36:50.10	14:01.11	2.46	24.58	0.07
36:50.15	12:16.9	0.905	23.06	273	36:50.16	12:16.99	0.69	22.47	−0.11
36:50.19	12:39.8	0.474	20.43	477	36:50.21	12:39.74	0.42	20.67	−0.04
36:50.20	13:41.7	1.249	24.10	883	36:50.19	13:41.84	1.39	24.87	0.06
36:50.26	12:45.7	0.680	21.74	524	36:50.26	12:45.78	0.58	21.45	−0.06
36:50.34	14:18.5	0.819	23.41	1028	36:50.36	14:18.65	0.85	23.09	0.02
36:50.48	13:16.1	0.851	23.07	749	36:50.47	13:16.12	0.90	22.60	0.03
36:50.82	12:55.8	0.321	22.27	611	36:50.82	12:55.89	0.41	22.55	0.07
36:50.83	12:51.5	0.485	23.15	563	36:50.84	12:51.47	0.56	23.16	0.05
36:51.04	13:20.6	0.199	19.38	757	36:51.05	13:20.69	0.11	19.60	−0.07
36:51.17	13:48.7	3.162	25.21	897	36:51.20	13:48.77	2.94	25.22	−0.05
36:51.37	14:20.9	0.439	23.22	1022	36:51.39	14:20.91	0.45	23.31	0.01
36:51.40	13:00.6	0.090	22.89	637	36:51.42	13:00.63	0.07	22.76	−0.02
36:51.69	12:20.2	0.401	21.45	257	36:51.71	12:20.17	0.43	21.56	0.02
36:51.77	13:53.7	0.557	21.08	912	36:51.79	13:53.81	0.57	21.10	0.01
36:51.96	13:32.1	1.087	23.59	801	36:51.97	13:32.17	0.97	23.12	−0.06
36:51.96	14:00.7	0.559	23.03	938	36:51.98	14:00.82	0.53	23.03	−0.02
36:51.99	12:09.6	0.458	22.75	138	36:52.01	12:09.67	0.53	22.90	0.05
36:52.40	13:37.7	3.430	25.08	824	36:52.41	13:37.75	3.75	24.79	0.07
36:52.66	12:19.7	0.401	23.11	220	36:52.67	12:19.69	0.51	23.20	0.08
36:52.72	13:54.7	1.355	21.85	904	36:52.74	13:54.77	1.43	21.98	0.03
36:52.73	13:39.1	3.369	25.03	825	36:52.75	13:39.07	3.49	25.07	0.03
36:52.84	14:04.8	0.498	23.45	941	36:52.87	14:04.86	0.63	23.27	0.09
36:52.86	14:08.2	3.367	24.49	957	36:52.98	14:08.47	3.48	26.85	0.03+
36:53.16	13:22.6	2.489	24.53	742	36:53.18	13:22.72	2.85	24.83	0.10
36:53.41	13:29.3	2.991	24.64	762	36:53.43	13:29.41	3.49	24.60	0.13
36:53.43	12:34.3	0.560	22.78	335	36:53.44	12:34.26	0.52	22.81	−0.03
36:53.59	14:10.1	3.181	24.78	955	36:53.59	14:10.15	3.72	24.55	0.13
36:53.65	14:17.6	0.517	23.36	979	36:53.65	14:17.62	0.45	23.45	−0.04
36:53.88	12:54.0	0.642	20.95	500	36:53.90	12:54.00	0.65	20.89	0.00
36:54.07	13:54.2	0.851	22.72	884	36:54.09	13:54.34	1.00	22.44	0.08
36:54.59	13:41.3	2.419	25.20	806	36:54.62	13:41.31	2.40	25.27	−0.01
36:54.70	13:14.8	2.232	24.15	670	36:54.72	13:14.77	2.41	24.29	0.06
36:54.96	13:14.8	0.511	23.81	662	36:55.00	13:14.78	0.55	23.81	0.03
36:55.06	13:47.3	2.233	24.23	831	36:55.06	13:47.06	2.40	24.52	0.05
36:55.11	13:11.3	0.321	23.58	631	36:55.14	13:11.38	0.27	23.61	−0.04
36:55.14	13:03.7	0.952	24.29	549	36:55.15	13:03.61	0.73	23.59	−0.11
36:55.39	13:11.0	0.968	22.86	619	36:55.45	13:11.19	0.87	22.16	−0.05
36:55.49	14:02.6	0.564	23.08	899	36:55.50	14:02.69	0.68	22.94	0.07
36:55.51	13:53.3	1.147	22.85	858	36:55.52	13:53.41	1.05	22.59	−0.05
36:55.55	13:59.8	0.559	23.74	888	36:55.58	13:59.88	0.64	23.70	0.05
36:55.59	12:46.2	0.790	23.08	381	36:55.57	12:45.48	0.90	21.93	0.06
36:55.59	12:49.3	0.950	23.53	409	36:55.62	12:49.27	0.94	22.99	−0.01
36:56.08	12:44.7	4.022	24.94	359	36:56.12	12:44.68	3.85	25.48	−0.03
36:56.10	13:29.6	0.271	23.80	734	36:56.12	13:29.66	1.07	23.39	0.63*

TABLE 2—*Continued*

Cohen *et al.* 2000				Fernández-Soto *et al.* 1999					
RA(−12h)	Dec(−62°)	$z_{\rm spec}$	R	ID	RA(−12h)	Dec(−62°)	$z_{\rm phot}$	$AB(8140)$	$\Delta z/(1+z)$[a]
36:56.39	12:09.3	0.321	23.22	11	36:56.42	12:09.23	0.43	23.27	0.08
36:56.61	12:20.1	0.930	23.15	104	36:56.65	12:20.14	0.76	22.57	−0.09
36:56.61	12:52.7	1.231	23.64	416	36:56.59	12:52.69	0.96	23.95	−0.12
36:56.62	12:45.5	0.518	20.06	345	36:56.64	12:45.32	0.69	20.00	0.11
36:56.89	13:01.5	0.474	23.69	486	36:56.92	13:01.58	1.27	23.03	0.54^{*}
36:56.90	12:58.0	0.520	23.84	454	36:56.93	12:58.19	0.58	23.59	0.04
36:57.18	12:25.9	0.561	22.36	144	36:57.21	12:25.81	0.63	22.39	0.04
36:57.27	12:59.5	0.475	21.07	458	36:57.31	12:59.65	0.49	21.32	0.01
36:57.49	12:11.0	0.665	21.10	1	36:57.47	12:10.56	0.71	21.20	0.03
36:57.51	12:12.1	0.561	22.62	6	36:57.44	12:11.88	0.71	23.28	0.10^{+}
36:57.69	13:15.3	0.952	22.94	599	36:57.71	13:15.19	0.86	23.02	−0.05
36:58.04	13:00.4	0.320	22.04	445	36:58.07	13:00.40	0.41	22.37	0.07
36:58.35	12:14.1	1.020	23.79	4	36:58.30	12:14.12	1.05	23.29	0.01
36:58.63	12:21.8	0.682	23.40	54	36:58.65	12:21.71	0.73	23.36	0.03
36:58.73	12:52.4	0.321	20.99	350	36:58.76	12:52.35	0.27	21.27	−0.04
36:59.01	12:23.7	4.050	25.33	60	36:59.10	12:23.59	4.10	25.28	0.01
36:59.41	12:21.5	0.472	23.53	33	36:59.37	12:21.65	0.45	24.04	−0.01
36:59.90	12:19.0	5.340	26.10	3	36:59.79	12:18.66	5.26	25.69	−0.01
37:00.05	12:25.3	2.050	23.83	48	37:00.08	12:25.23	2.30	23.77	0.08
37:00.53	12:34.7	0.563	21.43	125	37:00.56	12:34.61	0.44	21.37	−0.08

[a]A cross marks those objects with possible double identifications listed in Table 1. An asterisk marks the objects which are discussed in more detail in Sections 4 and 5.

TABLE 3

OBJECTS IN COHEN ET AL. (2000) WITH NO SPECTROSCOPIC REDSHIFT[a]

Cohen *et al.* 2000				Fernández-Soto *et al.* 1999				
RA(−12h)	Dec(−62°)	$z_{\rm spec}$	R	ID	RA(−12h)	Dec(−62°)	$z_{\rm phot}$	$AB(8140)$
36:39.8	12:29[b]	—	23.2	669	36:39.77	12:28.53	0.00	23.72
36:39.8	12:29[b]	—	23.2	678	36:39.71	12:29.60	1.14	24.27
36:45.3	11:43	—	24.0	81	36:45.29	11:42.89	0.70	23.94
36:47.2	13:42	—	23.9	917	36:47.17	13:41.88	1.16	23.72
36:48.5	13:17	—	23.4	775	36:48.47	13:16.64	0.27	23.29
36:52.6	12:02[c]	—	23.4	—	36:52.56	12:01.62	0.02	23.52
36:53.0	13:44[b]	—	24.0	852	36:53.02	13:44.21	2.28	24.60
36:53.0	13:44[b]	—	24.0	851	36:52.96	13:43.97	1.79	25.17
36:53.3	12:22[b]	—	23.7	237	36:53.25	12:22.72	0.77	25.02
36:53.3	12:22[b]	—	23.7	212	36:53.43	12:21.50	0.01	23.78

[a]One object in Table 10 in C00 (HDF36378_1235) does not enter our definition of the "HDF proper" area

[b]Two objects in our catalog correspond to one position as listed by C00

[c]Not an object in FLY99. See text for explanation

TABLE 4
PHOTOMETRY FOR OBJECT HDF36526_1202[a]

Magnitude AB(8140)	Flux(Error) F300W	Flux(Error) F450W	Flux(Error) F606W	Flux(Error) F814W	Flux(Error) J	Flux(Error) H	Flux(Error) K
23.52	81.36(10.35)	384.0(5.2)	834.4(3.6)	1429.0(6.0)	1934.0(177.5)	1617.0(300.5)	1739.0(252.9)

[a]All fluxes are in nJy

TABLE 5

STATISTICAL PROPERTIES OF THE $z_{\rm spec}$−$z_{\rm phot}$ COMPARISON

Redshift	Before corrections				After corrections			
range	$N_{\rm pts}$	$\langle \Delta z/(1+z) \rangle$	$\sigma_{\Delta z/(1+z)}$	% discordant	$N_{\rm pts}$	$\langle \Delta z/(1+z) \rangle$	$\sigma_{\Delta z/(1+z)}$	% discordant
0.0–1.5	113	0.0010	0.063	6.2	109	0.0003	0.063	0.0
1.5–4.0	27	0.0160	0.076	7.4	26	0.0186	0.068	0.0
4.0–6.0	6	−0.0045	0.016	0.0	6	−0.0045	0.016	0.0
0.0–6.0	146	0.0035	0.065	6.2	141	0.0035	0.064	0.0

TABLE 6

PROPERTIES OF THE OBJECTS WITH DISCORDANT REDSHIFTS

Name	$z_{\rm spec}$	R	Q[a]	$z_{\rm phot}$	Notes
HDF36386_1234	0.904	24.04	9	0.15	Inconclusive evidence (confusion with nearby object?)
HDF36396_1230	0.943	24.40	7	3.40	$z = 3.475$ must be the real value
HDF36409_1205	0.882	22.94	9	0.00	Inconclusive evidence (confusion with nearby object?)
HDF36414_1143	0.548	23.51	3	1.32	Inconclusive evidence (confusion with nearby object?)
HDF36441_1410	2.267	24.26	1	0.01	$z = 0.065$ must be the real value
HDF36450_1251[b]	2.801	24.37	3	2.23	F300W excess. $z_{\rm spec}$ unlikely
HDF36478_1256	2.931	24.35	2	0.26	$z_{\rm spec}$ must be right
HDF36494_1317	0.271	23.63	3	1.24	$z = 1.238$ must be the real value
HDF36561_1330	0.271	23.80	4	1.07	$z = 1.238$ must be the real value
HDF36569_1302	0.474	23.69	1	1.27	$z_{\rm spec}$ wrong due to nearby object.

[a]Spectroscopic quality flag assigned by C00. See text for details

[b]This object is not $> 4\sigma$-discordant, but strong evidence points to the spectroscopic redshift being in error. See text for details

Fig. 1.— Comparison of spectroscopic and photometric redshifts for the 146 objects in the sample. The large squares mark those points which are discordant at a level $> 4\sigma$.

Fig. 2.— Comparison of spectroscopic and photometric redshifts for the 146 objects in the sample. Symbols are as in Figure 1. The dashed lines mark the 1σ interval and the mean value of $\Delta z/(1+z)$ for the sample as a whole.

Fig. 3.— Distribution of the residuals from the $z_{\rm spec}$–$z_{\rm phot}$ comparison. The dotted line is a gaussian distribution with mean=0.0035, $\sigma = 0.065$.

Fig. 4.— (a–j)Spectral energy distributions of the different models at $z_{\rm spec}$ (upper panels) and of our best-fit model at $z_{\rm phot}$ (mid panel, empty circles mark the expected flux for each filter), compared to the observed photometry (points with error bars). The bottom panel in each figure shows the likelihood function and the values of $z_{\rm spec}$, $z_{\rm phot}$, and our best-fit type.

Fig. 5.— F814W images of all the objects discussed in detail in Sections 3 and 4. The size of each image is 8x8 arcsec.

Fig. 6.— Comparison of spectroscopic and photometric redshifts for the 141 objects in the final sample, after the discordant values have been individually checked. The large square and two error bars joined by a dotted line correspond to the 2σ confidence interval around the $z_{\rm phot}$ value as calculated for HDF36478_1256.

Fig. 7.— Comparison of spectroscopic and photometric redshifts for the 141 objects in the final sample. Symbols are as in Figure 6. The dashed lines mark the 1σ interval and the mean value of $\Delta z/(1+z)$ for the sample as a whole.

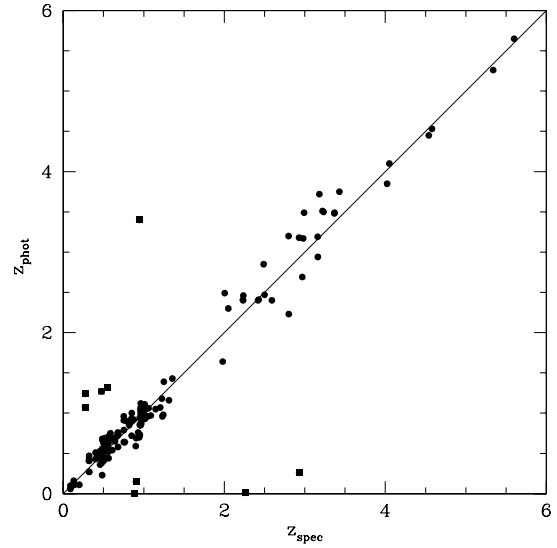

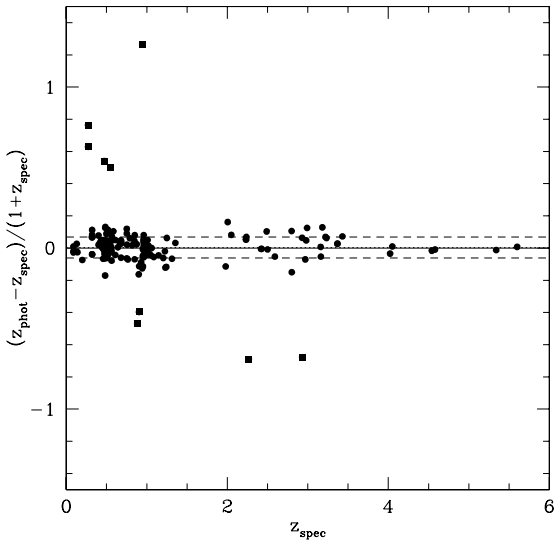

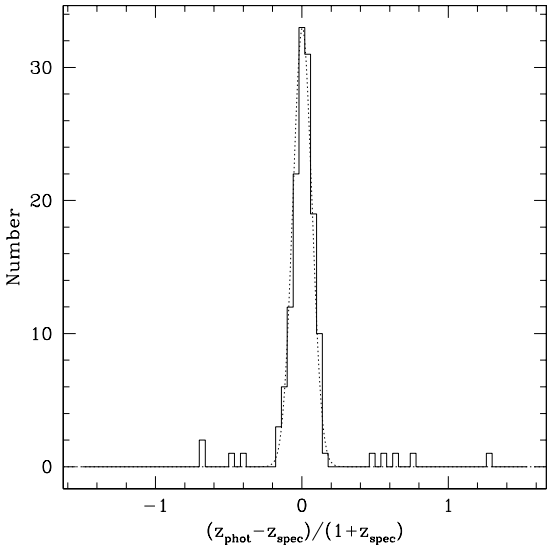
Number
$(z_{phot}-z_{spec})/(1+z_{spec})$

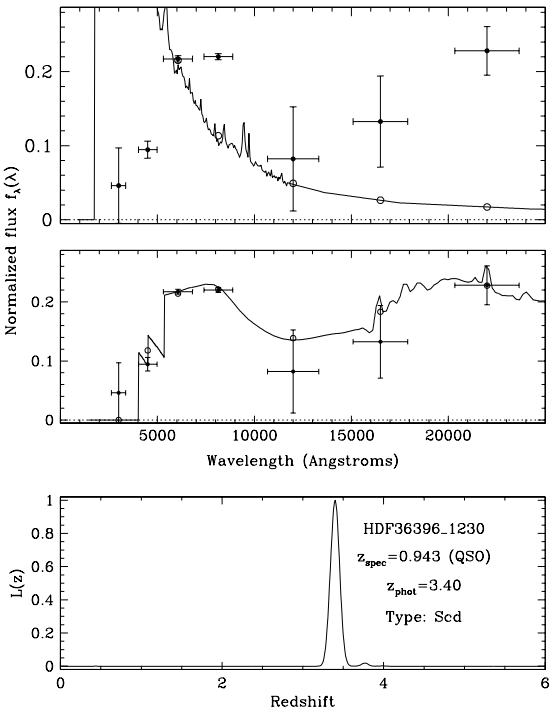
Normalized flux $f_\lambda(\lambda)$
Wavelength (Angstroms)
L(z)
Redshift
HDF36396_1230
z_{spec}=0.943 (QSO)
z_{phot}=3.40
Type: Scd

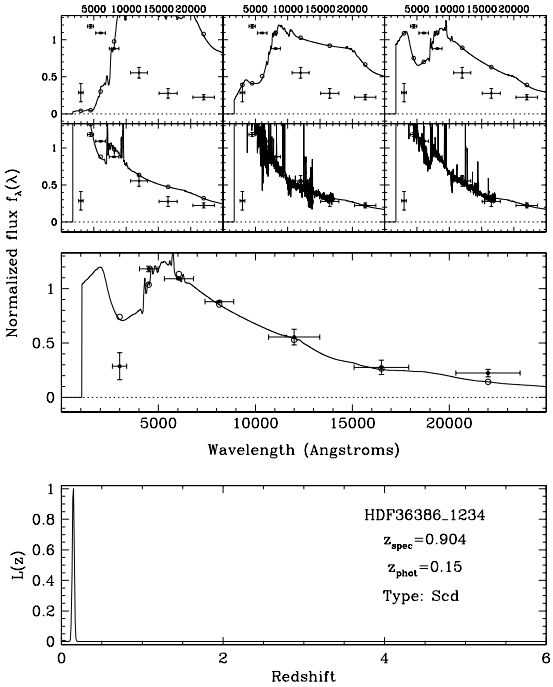
Normalized flux $f_\lambda(\lambda)$
Wavelength (Angstroms)
L(z)
Redshift
HDF36386_1234
z_{spec}=0.904
z_{phot}=0.15
Type: Scd

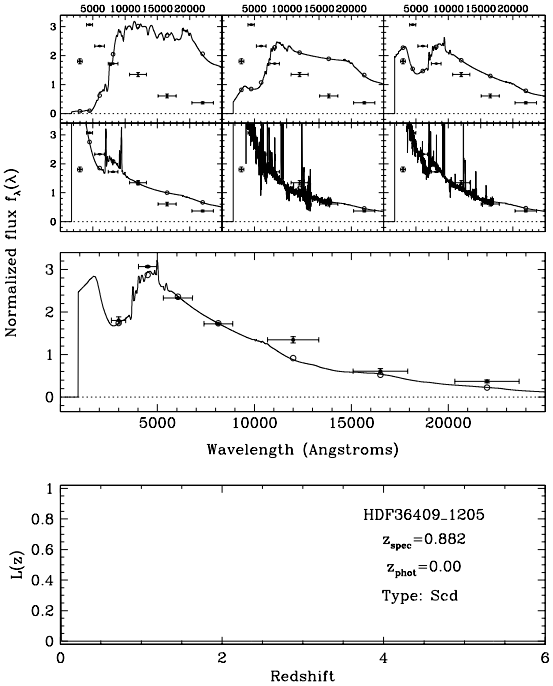
Normalized flux $f_\lambda(\lambda)$
Wavelength (Angstroms)
L(z)
Redshift
HDF36409_1205
z_{spec}=0.882
z_{phot}=0.00
Type: Scd

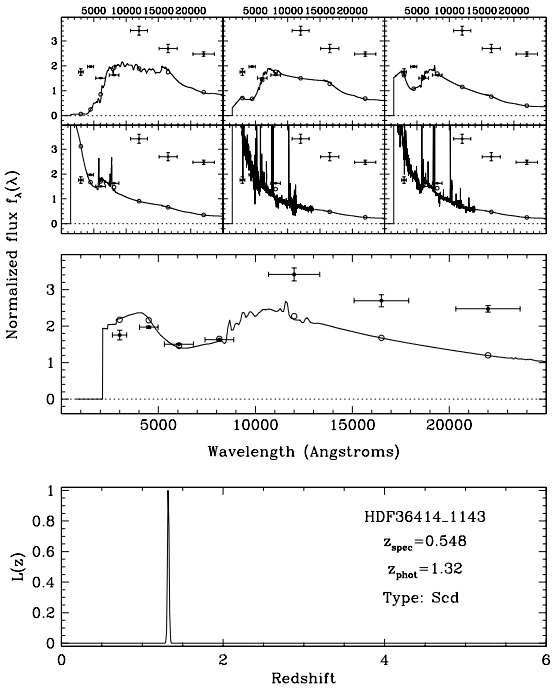
Normalized flux $f_\lambda(\lambda)$
Wavelength (Angstroms)
L(z)
Redshift
HDF36414_1143
z_{spec}=0.548
z_{phot}=1.32
Type: Scd

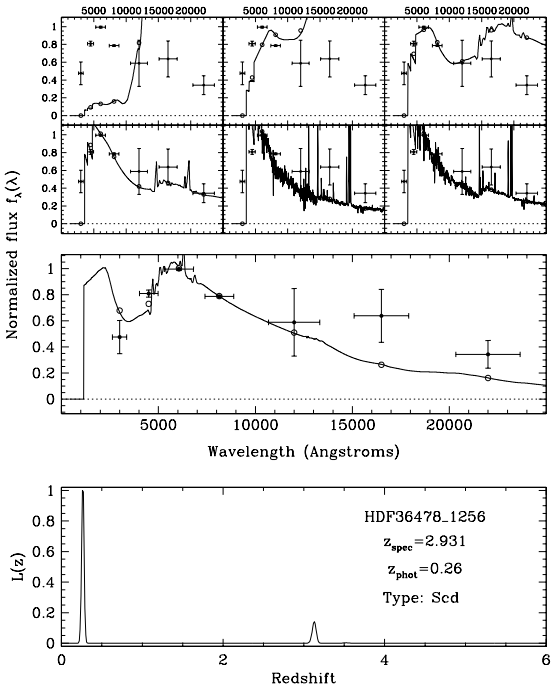
Normalized flux $f_\lambda(\lambda)$
Wavelength (Angstroms)
L(z)
Redshift
HDF36478_1256
z_{spec}=2.931
z_{phot}=0.26
Type: Scd

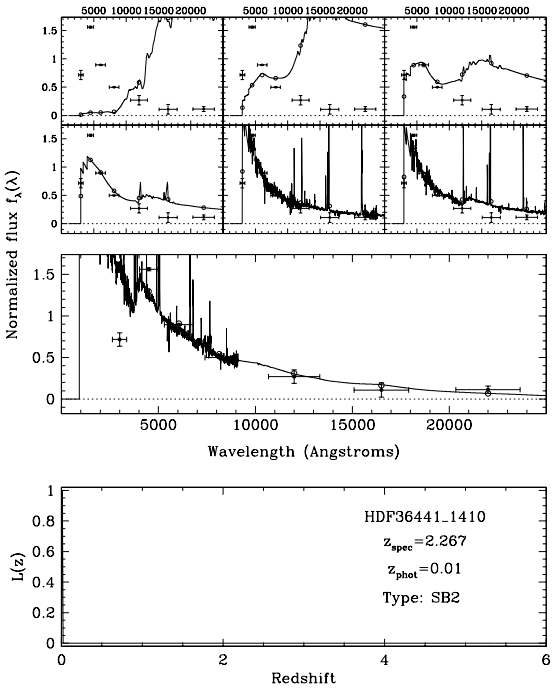
Normalized flux $f_\lambda(\lambda)$
Wavelength (Angstroms)
L(z)
Redshift
HDF36441_1410
z_{spec}=2.267
z_{phot}=0.01
Type: SB2

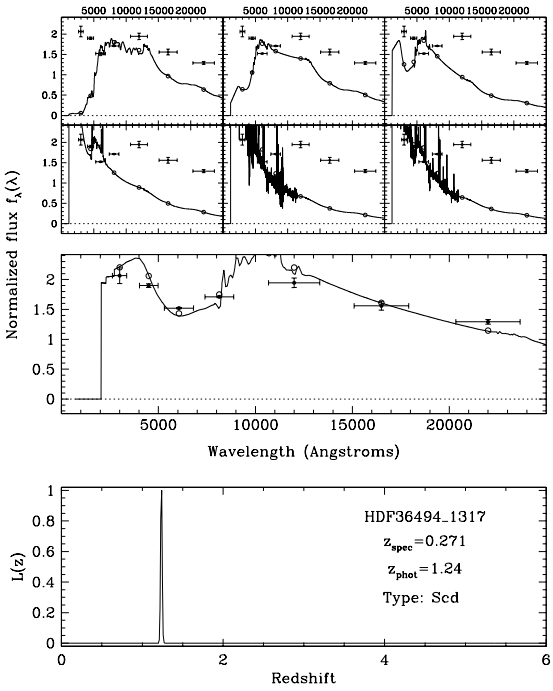
Normalized flux $f_\lambda(\lambda)$
Wavelength (Angstroms)
L(z)
Redshift
HDF36494_1317
z_{spec}=0.271
z_{phot}=1.24
Type: Scd

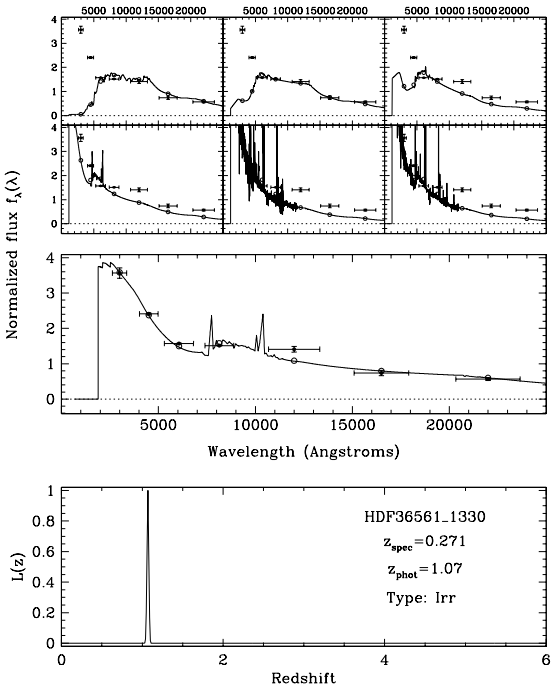
Normalized flux $f_\lambda(\lambda)$
Wavelength (Angstroms)
L(z)
Redshift
HDF36561_1330
z_{spec}=0.271
z_{phot}=1.07
Type: Irr

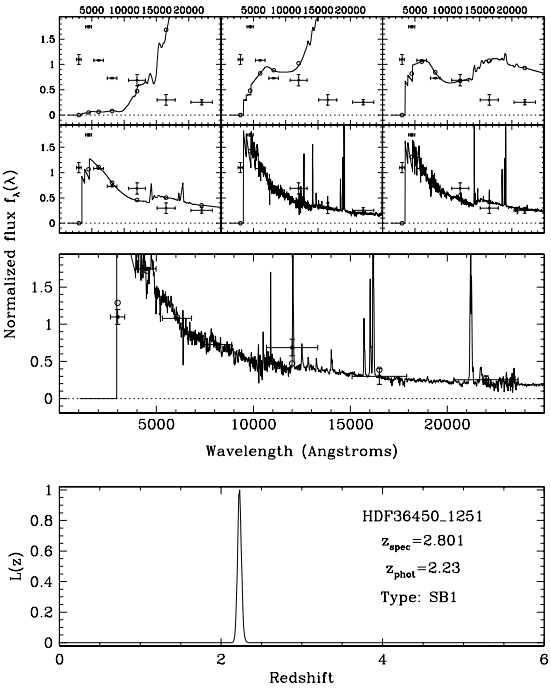
Normalized flux $f_\lambda(\lambda)$
Wavelength (Angstroms)
L(z)
Redshift
HDF36450_1251
z_{spec}=2.801
z_{phot}=2.23
Type: SB1

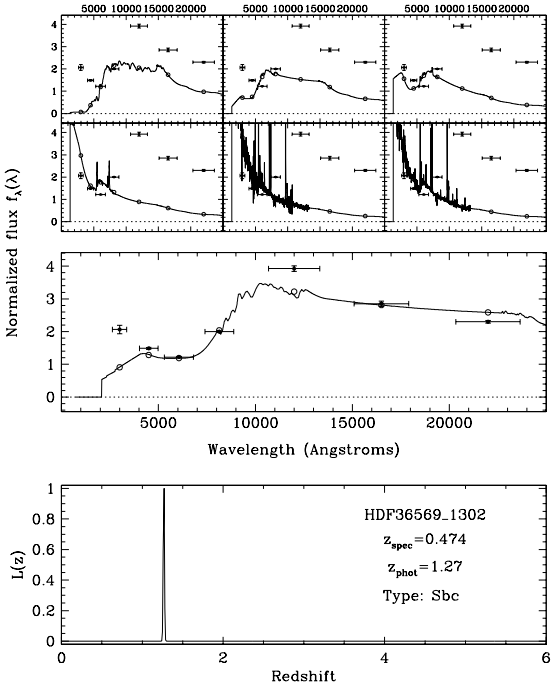
Normalized flux $f_\lambda(\lambda)$
Wavelength (Angstroms)
L(z)
Redshift
HDF36569_1302
z_{spec}=0.474
z_{phot}=1.27
Type: Sbc

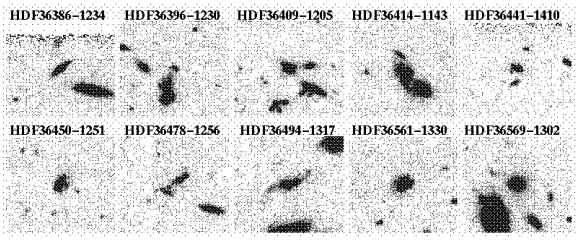
HDF36386−1234
HDF36396−1230
HDF36409−1205
HDF36414−1143
HDF36441−1410
HDF36450−1251
HDF36478−1256
HDF36494−1317
HDF36561−1330
HDF36569−1302

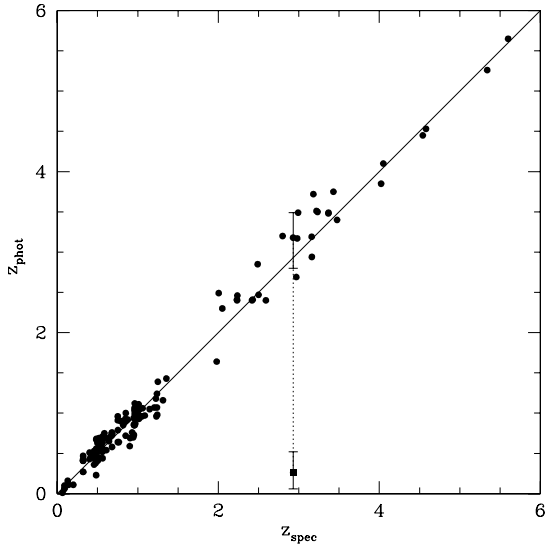
6
4
2
0
0
2
4
6
z_{phot}
z_{spec}

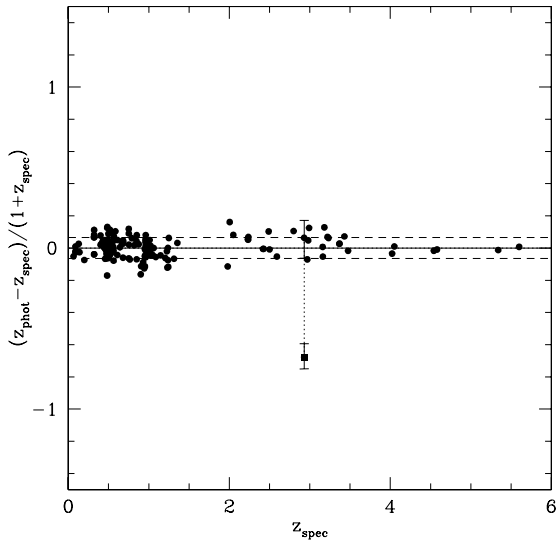
1
0
−1
0
2
4
6
$(z_{phot}-z_{spec})/(1+z_{spec})$
z_{spec}